Evaluation of preparation and combustion rig tests of an effusive cooled SiC/SiCN panel

Sandrine Hönig, Fabia Süß, Neraj Jain, Raouf Jemmali, Thomas Behrendt, Bernd Mainzer, Dietmar Koch

Angaben zur Veröffentlichung / Publication details:

Hönig, Sandrine, Fabia Süß, Neraj Jain, Raouf Jemmali, Thomas Behrendt, Bernd Mainzer, and Dietmar Koch. 2020. "Evaluation of preparation and combustion rig tests of an effusive cooled SiC/SiCN panel." *International Journal of Applied Ceramic Technology* 17 (4): 1562–73. https://doi.org/10.1111/ijac.13501.

Received: 29 November 2019 | Revised: 3 February 2020 | Accepted: 3 March 2020

DOI: 10.1111/ijac.13501

International Journal of Applied Ceramic Technology

SPECIAL ISSUE ARTICLE

Evaluation of preparation and combustion rig tests of an effusive cooled SiC/SiCN panel

Sandrine Hönig[1] | **Fabia Süß**[1] | **Neraj Jain**[1] | **Raouf Jemmali**[1] | **Thomas Behrendt**[2] | **Bernd Mainzer**[3] | **Dietmar Koch**[4]

[1]German Aerospace Center (DLR), Institute of Structures and Design (BT), Stuttgart, Germany

[2]German Aerospace Center (DLR), Institute of Propulsion Technology (AT), Cologne, Germany

[3]Morgan Advanced Materials Haldenwanger GmbH, Waldkraiburg, Germany

[4]Chair of Materials Engineering, University of Augsburg, Augsburg, Germany

Correspondence
Sandrine Hönig, German Aerospace Center (DLR), Institute of Structures and Design (BT), Stuttgart, Germany.
Email: sandrine.hoenig@dlr.de

Abstract

SiC/SiCN ceramic matrix composites (CMCs) are promising candidates for components of aero-engines. To evaluate the properties of these CMCs under realistic conditions, a quasi-flat panel with effusion cooling holes was investigated in a high pressure combustor rig. A Tyranno SA3 fabric-based SiC/SiCN composite with high strength and strain to failure was manufactured via polymer infiltration and pyrolysis process. Due to its weak matrix no fiber coating was necessary for damage tolerant behavior. The cooling holes in the panel were introduced via laser drilling. An outer coating of CVD-based SiC was finally applied for enhanced oxidation resistance. The specimen was tested in the combustor rig and the cooling effectiveness was evaluated. The microstructure of laser machined holes was studied via microscopy and energy-dispersive X-ray spectroscopy. The macrostructure was investigated via computing tomography scans before and after the combustor test. Material performances at higher temperatures were estimated via a material performance index. Local microstructure modifications were observed after laser drilling. No crack formation was observed in the CMC panels after rig tests. The measured global cooling effectiveness of 0.76 and the analytical performance evaluation demonstrate the potential benefit of SiC/SiCN materials in combustor applications.

KEYWORDS

ceramic matrix composites, heat engines, lasers, SiC/SiCN, silicon carbide, X-ray computed tomography

1 | INTRODUCTION

Improving environmental performances and efficiency of aircraft engines is essential for answering the increase of global aircraft traffic of 4.4% per year predicted by the industry.[1] In this regard, new gas turbine technologies like combustor components based on high temperature ceramic matrix composites (CMCs) are developed since the 1990s.[2–5]

In almost all aero gas turbines combustion occurs in a rich lean staged combustor. At the upstream end of the combustor an air fuel mixture with a fuel-rich equivalence ratio is injected and combustion is stabilized by recirculated hot combustion products. This ensures stable combustion over the full operational envelope of the engine. Further downstream additional air is injected into the combustor in order to complete fuel oxidation. Typical flame temperatures are

in excess of 2000 K requiring efficient air cooling of the combustor walls. At the combustor outlet the mixture has a fuel-lean equivalence ratio to match the required inlet conditions of the turbine. During the transition from fuel-rich to fuel-lean, stoichiometric regions with the highest temperatures are inherently present leading to peak production rates of nitric oxides (considered as a pollutant). To increase the fuel efficiency of the engine, temperatures and pressures must be increased in the combustor. This will result in further increasing of the production of nitric oxides. The most promising approach to solve this design conflict is the lean combustion as introduced by the General Electric GEnX engine.[6] Lean combustion requires a completely different air flow distribution into the combustor resulting in a significantly reduced amount of air available for cooling. CMCs promising higher service temperatures are an interesting alternative to super alloys, see Ref.[7] In the past, there had been a number of approaches to develop and test non-oxide CMC combustors for aero-engine applications. For lower engine pressure ratios the CMC combustors were designed to run without any active cooling film.[8,9] With the anticipated gas temperatures in future fuel efficient and high overall pressure ratio engines, for example, General Electric GE9X,[10] even high temperature CMCs may have to rely on active cooling films.[11] Experimental investigations with an effusion-cooled five-sector CMC combustor are reported in Ref.[11]

Non-oxide CMCs exhibit high specific strength at elevated temperatures as well as a high strain to failure and thermal shock resistance.[12,13] Silicon carbide fiber reinforced composites were developed in the past 30 years. Such composites, like SiC/SiC have found their application in jet engines as shroud material and are of high interest for next generation nuclear reactors.[3,14,15] The three most common routes to infiltrate the matrix of non-oxide CMCs are polymer infiltration and pyrolysis (PIP), chemical vapor infiltration and liquid silicon infiltration. PIP is a rather simple process based on the infiltration of preceramic silicon-based organo-substituted polymers into fiber prepregs and subsequent pyrolysis.[16] Thereby, the precursor is transformed by decomposition to an amorphous or crystalline ceramic, depending on the chosen temperature.[17,18] As precursor, a polysilazane based resin is chosen. In the amorphous state, polysilazanes generate a high volume yield and thereby, they allow the manufacture of comparably cheap PIP based CMCs. Recently, it was shown that at room temperature such SiC/SiCN composites based on Tyranno SA3 fibers achieve a high strength and high strain to failure, even without fiber coating.[17]

Laser machining is a rapid technology with high level of reproducibility for bringing cooling holes into a CMC component. Effects from machining of monolithic SiC via diverse laser technologies were reported by Lippmann et al, Fu et al and Li et al.[19–21] Buildup of thin glass phase or SiO_2 amorphous layer on SiC surface was stated. By laser-supported joining of SiC/SiCN, Herrmann et al[22] reported the buildup of SiO_2 phase on CMC components. Nevertheless no detailed studies of the SiO_2 microstructure were presented in these works.

One key issue for the implementation of a material in an aircraft engine is a confident prediction of its in-service performance at high temperature. Moreover the number of materials available for application is high and it can become a challenging task for design engineers to finalize the materials at the initial stage of component design. The selection becomes more difficult with CMCs because of their anisotropic nature. Some criteria and methods have already been proposed in the literature to compare the materials based on their properties but they are rather general in nature and do not consider the temperature dependency of material properties, which are crucial for application under consideration.[23,24]

DLR is developing a temperature-dependent material performance index (MPI) to facilitate preliminary selection of alloys and CMCs specific to cylindrical components under thermal stresses; like for instance combustor liners and turbine elements of aero-engines.

Only few experimental evaluations of film cooling hole for SiC/SiC combustor liners are reported in the literature.[7,25] Cooling effectiveness of 3D woven SiC/SiC structures was experimentally analyzed by Zhong et al[25] and numerically by Mehta et al.[26] Many cooling investigations are conducted under non-reacting conditions like in the grouping of test rigs in Ref.[25] These investigations typically lack a realistic swirling and highly turbulent hot gas flow. The cooling effectiveness of 2D laminated SiC/SiCN component under realistic hot gas flow is investigated in this paper and fills in the scientific literature. Moreover the MPI of SiC/SiCN composite will be evaluated for the first time in the present work.

The objective of this paper was to evaluate the in-service performance of SiC/SiCN materials for combustor applications. A quasi-flat panel with effusion cooling holes was investigated in a high pressure combustor rig. A Tyranno SA3 fabric based SiC/SiCN composite was manufactured via PIP process. Due to its weak matrix no fiber coating was necessary for damage tolerant behavior. The cooling holes in the panel were introduced via laser drilling. An outer coating of CVD-based SiC was finally applied for enhanced oxidation resistance.

The microstructure of laser machined holes was studied via microscopy and energy-dispersive X-ray spectroscopy. The cooling effectiveness of the specimen was evaluated in the cooling rig facility. The macrostructure was examined via computed tomography scans before and after the combustor test. Material performances at higher temperatures were evaluated via a MPI.

2 | MATERIALS, EXPERIMENTAL METHODS AND ANALYTICS

2.1 | Material

The SiC/SiCN composites were manufactured by the PIP process (Figure 1). It is a two-stage cycled process, beginning with the infiltration of a SiC fiber-preform composed of Tyranno SA3 plain weave fabrics with a polysilazane (PSZ20, Clariant SE). Resin transfer molding was used as a production technique, which resulted in a dense SiC fiber-reinforced polymer. After thermal curing at 260°C, a subsequent pyrolysis converts the polymer matrix to a ceramic SiCN matrix. During pyrolysis at 1300°C, an amorphous, single-phase SiCN network was formed. The resulting evaporation of volatile compounds and the increase in density led to the evolution of porosity within the matrix. To improve the mechanical properties and oxidation resistance, a total of eight infiltration and pyrolysis cycles were performed. A plate with a final fiber volume content of 47 vol.-% was processed.

To determine the MPI for the SiC/SiCN composite the coefficient of thermal expansion ($CTE_{//}$) and the thermal conductivity ($\lambda_{//}$) along fiber direction are required. $CTE_{//}$ was measured in the range of 50°C-1300°C with a Netzsch DIL 402 E under argon atmosphere following standard DIN EN 1159-1. For evaluation of the thermal conductivity $\lambda_{//}$, the heat capacity and thermal diffusivity ($a_{//}$) should be measured. For measurement of the thermal diffusivity via standard laser flash method the manufacturer of machinery recommends a sample thickness of 12.7 mm transverse to the direction of measurement. Hence for experimental analysis of $a_{//}$, a plate with a thickness larger than 12.7 mm should be manufactured for realizing samples with required surface quality. Such a thick SiC/SiCN plate is cost expensive and couldn't be processed during this study. Therefore it was chosen to use values of $\lambda_{//}$ from comparable CMC found in literature.[22]

2.2 | Machining/coating

The principal machining features and specimen dimensions are described in Figure 2. In the first step, the manufactured SiC/SiCN plate was machined with a surface grinding machine. Then the test specimen was cut and three edges were milled with a CNC machine (Computerized Numerical Control). These edges are later pressed in the combustor test bench for fixation of the specimen. The final SiC/SiCN specimen outer dimensions are $51 \times 84 \times 3.6$ mm^3.

Effusive cooling holes and holes for thermocouples and their fixation systems were machined using a ND-YAG laser in air with a wavelength of 1064 nm. The pulse duration was adjusted specifically to the material, geometry, and atmospheric conditions. The specifications are a cooling hole diameter of 0.9 mm after laser drilling and a hole inclination at an angle of 25° relative to the specimen surface. The laser entered the specimen on the "hot" surface of the sample, that is, the surface that will be exposed to the hot gases during combustion tests. As a result, the wider diameter produced by laser entering should have limited effect over the cooling gas flow entering inside the effusive cooling holes.

In the final step, the specimen was coated with a SiC layer of 70-100 µm via chemical vapor deposition.

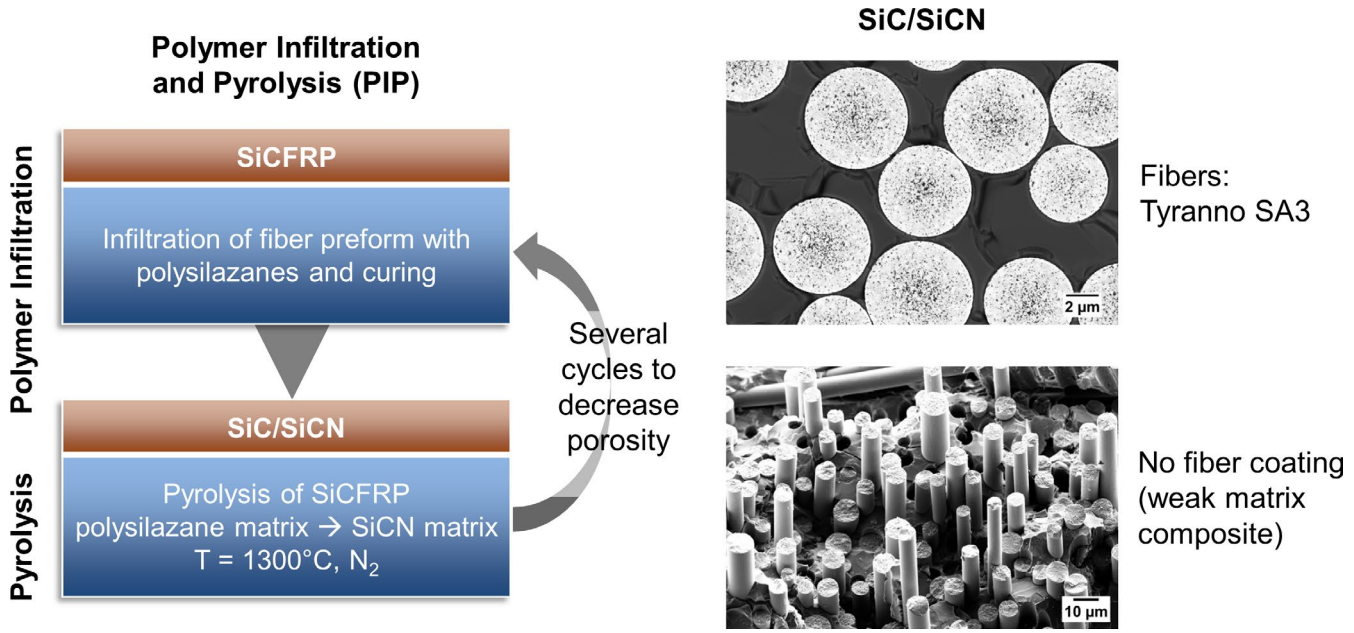

FIGURE 1 Manufacturing process of SiC/SiCN material, adapted from Ref.[31] [Color figure can be viewed at wileyonlinelibrary.com]

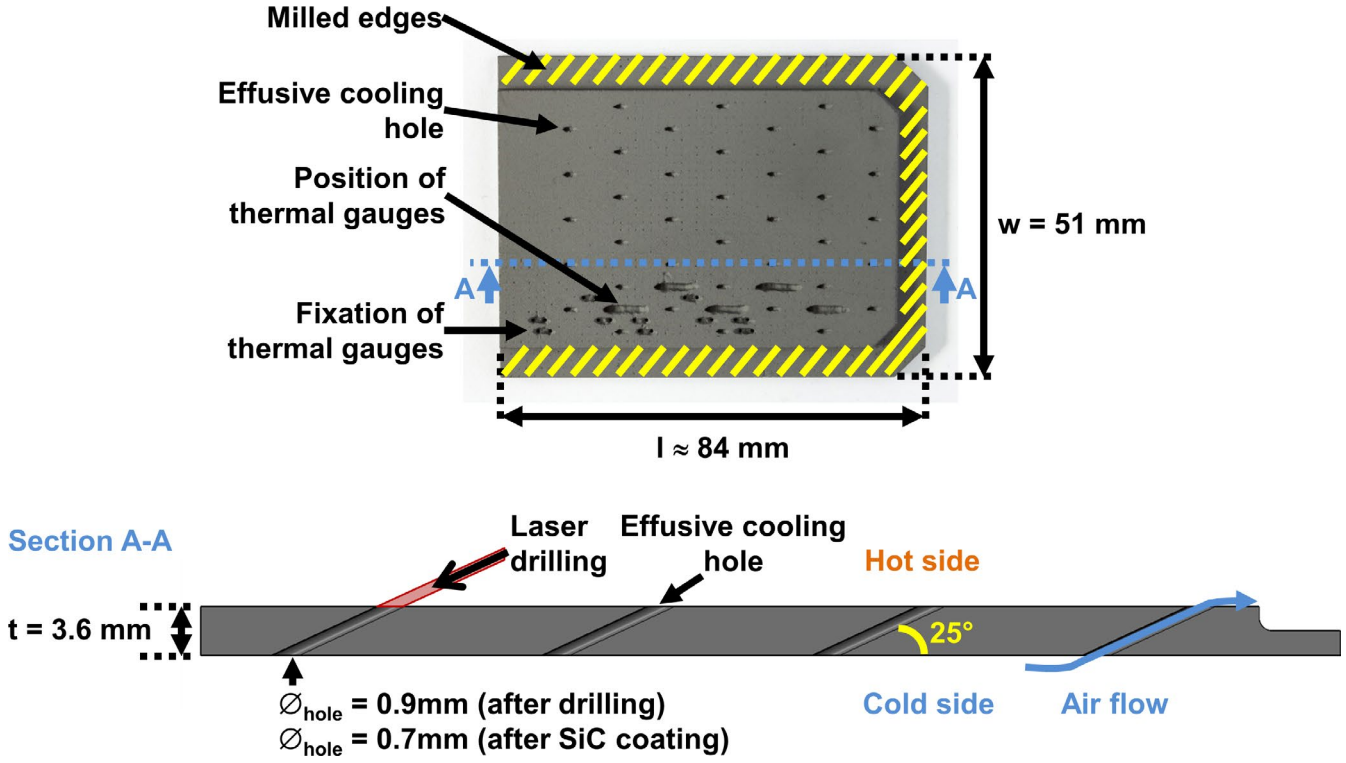

FIGURE 2 SiC/SiCN specimen dimensions and machining description [Color figure can be viewed at wileyonlinelibrary.com]

Laser drilling effects were investigated via computing tomography (CT), scanning electron microscope (SEM) and energy dispersive X-ray spectroscopy (EDX) analysis.

2.3 | Tests in high pressure cooling rig

The experiments were run in the high pressure cooling rig (HPCR) at DLR. A tubular water cooled combustor with a fuel-lean prototype burner running on kerosene served as a hot gas generator. Hot exhaust gases flew through the test section, which was located downstream of the combustor. The test sample was installed in a module in a sidewall of the test section. The velocity and temperature boundary layer caused by the convectively cooled liner walls was removed by means of a boundary layer bleed immediately upstream of the test sample. A more detailed description of the test rig is given in Ref.[27] The conditions of the hot gas flow, listed in Table 1, are laterally averaged values from detailed measurements reported in Ref.[27] The cooling air temperature was measured on the rear of the test sample and was kept constant at T_c = 470 K. The relative cooling air pressure drop, defined as the pressure drop of the cooling air across a test sample divided by the hot gas pressure, was varied in the range Δp_c = 2.1%-4%. The total cooling effectiveness was measured for this pressure drop range. The total cooling effectiveness is a non-dimensional temperature ranging from zero to one. An effectiveness of zero means that the wall temperature equals the hot gas temperature (no cooling at all) and an effectiveness of one means that the wall temperature equals the cooling air temperature (perfect cooling), see Equation 1.

TABLE 1 Operating conditions in the high pressure cooling rig

Combustor preheat temperature T_3	650 K
Combustor air to fuel ratio *AFR*	31.4
Pressure in test section p_h	5 bar
Hot gas velocity u_h in main flow direction near the wall	29.7 m/s
Turbulence level in hot gas flow *Tu*	22%
Hot gas temperature T_h near the wall	1560 K
Cooling air temperature test sample T_c	470 K
Relative cooling air pressure drop Δp_c	2.1%-4%

$$\eta_{tot} = \frac{T_{hot\ gas} - T_{wall}}{T_{hot\ gas} - T_{cool}} \quad (1)$$

The specimen was equipped with five thermocouples on the hot gas side. These temperature measurements were used in the in-situ calibration of the infrared camera, see Ref.[28]

Defects and structural modifications of the SiC/SiCN specimen due to combustion tests were analyzed via CT scans before and after tests.

The test presented in this contribution is not meant as a material endurance test on a specific temperature range but as a characterization of the cooling performance under realistic operating conditions.

2.4 | Material performance index

The thermomechanical stresses developed in a hollow cylinder under an axisymmetric temperature distribution were analytically evaluated for isotropic materials by Timoshenko.[29] Timoshenko proves the dependency of the radial, hoop and axial stresses from the factor $E \times \mathrm{CTE}$ where E is the Young's modulus.

It is obvious for combustor chamber component that a high thermal conductivity has a positive influence on the thermomechanical behavior by providing better conduction of cooling flows and limiting local thermal gradients and therefore thermal stresses.

A high tensile strength of material is another keypoint for material design.

All those previous statements can be summarized in one formula defining a MPI in cylindrical components under thermal loads, where properties with positive influence (σ_{yield} and λ) are placed at numerator position and the properties with negative influence (E_{tens} and CTE) are placed at denominator position.

For super alloys the MPI is given by:

$$\mathrm{MPI}(T) = \frac{\sigma_{\mathrm{yield}}(T) * (T)}{E_{\mathrm{tens}}(T) * \mathrm{CTE}(T)} \tag{2}$$

where MPI is the material performance index [W/m]; σ_{yield} is the yield strength [Pa] at 0.2% offset for alloys and 0.005% offset for CMC; λ is the thermal conductivity [W/(m K)]; E_{tens} is the Young's modulus [Pa]; CTE is the coefficient of thermal expansion [1/*K*]; *T* is the service temperature [°C].

For CMCs the MPI relies on the same equation, the properties are however respective to the fiber direction, which is assumed to be representative of the material behavior for the sake of simplicity. The yield strength is evaluated at 0.005% offset, this value relied on the strain offset used for the HiPerComp™ CMC.[30]

For easier comparison of the MPI a min-max normalization is done:

$$\mathrm{MPI}_{\mathrm{norm}} = \frac{\mathrm{MPI} - \mathrm{MPI}_{\mathrm{min}}}{\mathrm{MPI}_{\mathrm{max}} - \mathrm{MPI}_{\mathrm{min}}} \tag{3}$$

where $\mathrm{MPI}_{\mathrm{min}}$ and $\mathrm{MPI}_{\mathrm{max}}$ are respectively the minimum or maximum MPI of all analyzed materials.

The MPI of different alloys (Inconel 718, Inconel HX as well as the relatively new Haynes 282) typically used for combustor applications were evaluated for different temperatures based on the manufacturer's datasheets.

The MPI of the SiC/SiCN material was also estimated at different temperatures and relied on the following material properties. Tensile properties of SiC/SiCN material with a 70-100 µm CVD-SiC coating were characterized at room temperature in other work: a tensile modulus of 169 ± 14 GPa and a yield strength of 92 ± 25 MPa at 0.005% offset were experimentally measured. Mainzer et al proved that the tensile modulus of SiC/SiCN materials with Tyranno SA3 fibers kept constant after 10 hours of oxidation at 1200°C.[17] Moreover Mainzer et al demonstrated that the SiCN matrix is amorphous at temperatures up to 1500°C under nitrogen atmosphere[31]; above this temperature crystallization occurs. Tensile properties of Tyranno SA3 fibers kept constant up to 1800°C under inert gas atmosphere.[32] For these reasons it is assumed that if oxidation is prevented the tensile modulus and yield strength of SiC/SiCN keeps constant up to 1200°C. This temperature limit is therefore set for the evaluation of the MPI. $\mathrm{CTE}_{//}$ was measured during the present work (1.0-4.9 × 10^{-6}/K at 50°C-1200°C) and $\lambda_{//}$ was estimated via the work of Herrmann et al on comparable material[22]: 18.3-10.3 W/mK at 50°C-1400°C. No information about the behavior of $\lambda_{//}$ between 50°C and 1400°C is given, therefore a linear behavior is assumed. Herrmann et al measured an open porosity (>20 vol.-%) higher than that of the studied SiC/SiCN (4 vol.-%). So it can be assumed that the thermal conductivity of the investigated SiC/SiCN material should be higher than the values measured by Herrmann. Therefore, in this paper only a minimal potential MPI of the SiC/SiCN material is evaluated.

3 | RESULTS AND DISCUSSION

3.1 | Laser machining

The positions and geometries of the cooling holes were analysed via CT analysis and compared to the geometrical specifications (Figure 2). The position analysis reveals a standard deviation smaller than 0.1 mm, which is sufficient for guaranteeing the intended cooling flow. Some cooling holes show a slight conical geometry with a cone angle varying between 0° to about 2°. The surfaces of the cooling holes are inclined at angles of 25° ± 1° relative to the specimen surface. On the laser entering side, the hole presents a wider opening region (Figure 3) due to higher heat concentration at laser contact point. As located on the hot side of the sample; this has little effect on the cooling gas volumetric flow rate. A complete SiC coating of all surfaces was achieved including the inner side of the cooling hole (Figure 3) with a coating thickness of 50-100 µm, hence the oxidation resistance for the rig test is guaranteed. Under the SiC coating layer and inside the cooling holes the formation of a new phase was identified via CT analysis as shown on Figure 3.

Detailed investigations via SEM, EDX spectrum analyses of selected spots and micro-CT (Figures 4-7) show the formation of a porous SiO_2 layer of max. 80 µm after laser drilling, on one half of each cooling hole inner surface. The

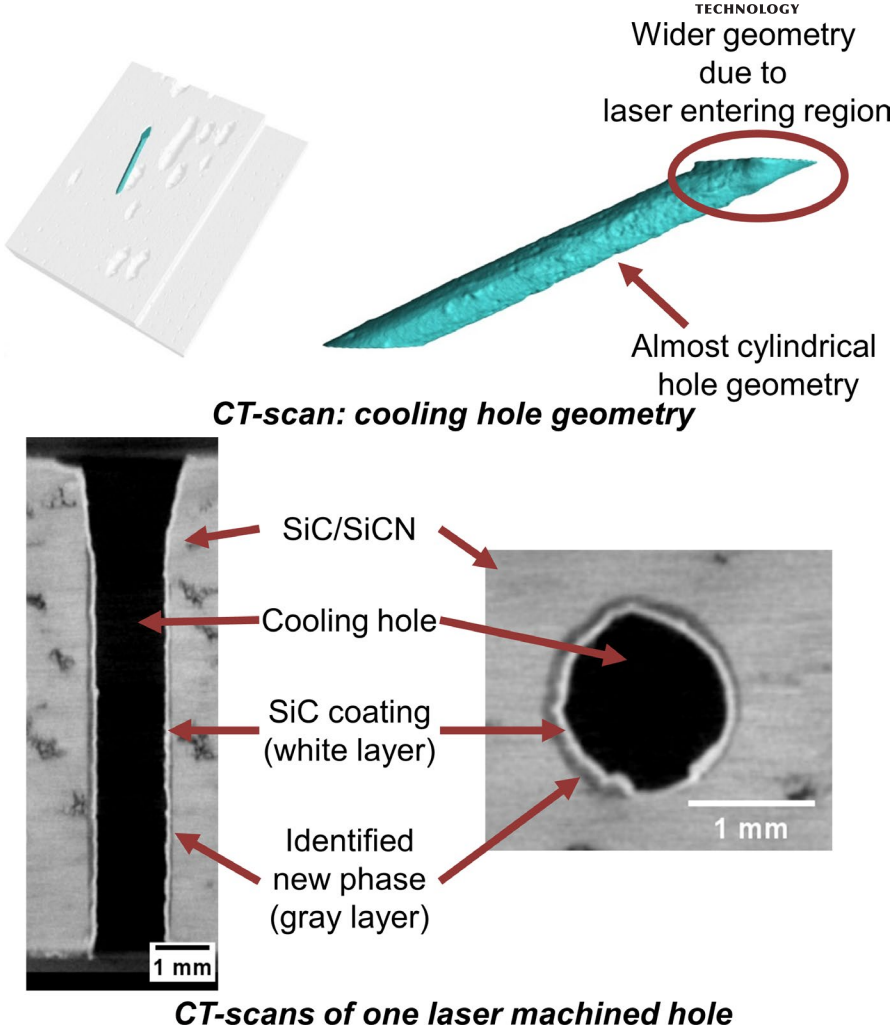

FIGURE 3 CT analysis of cooling hole geometry and microstructure. CT, computing tomography [Color figure can be viewed at wileyonlinelibrary.com]

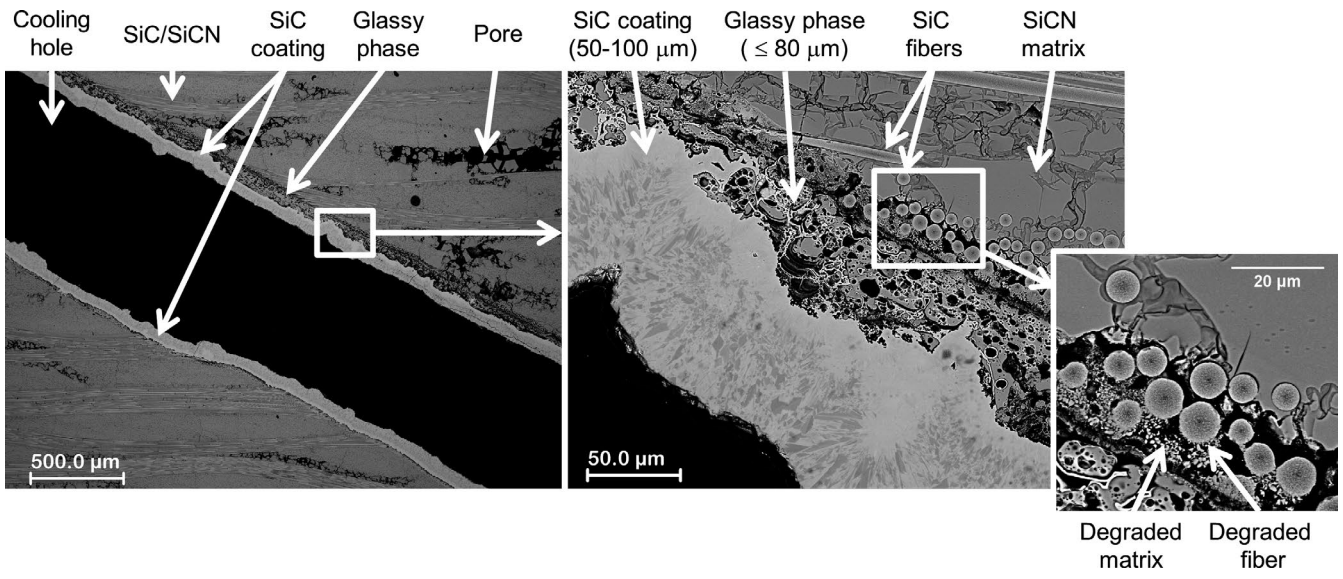

FIGURE 4 Microstructure analysis via SEM of cooling hole surface. SEM, scanning electron microscope

SiO_2 layer buildup induces local matrix and fiber degradations. The SiO_2 compound is stated via EDX investigations as 64 at.% oxygen is measured which is around the double atomic percentage of silicon with 30 at.%. A low presence of carbon (6 at.%) due to impurities introduced by the embedding resin was also measured.

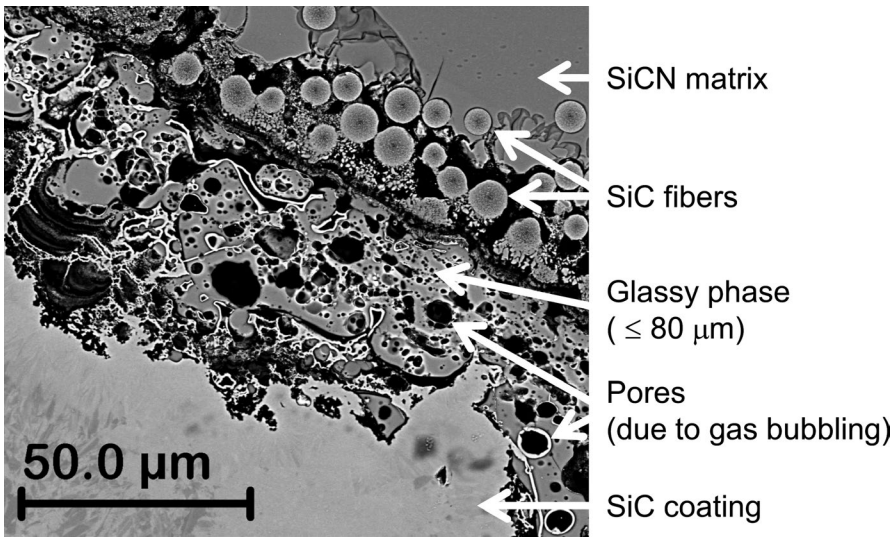

FIGURE 5 Microstructure analysis via SEM of the SiO_2 glassy phase. SEM, scanning electron microscope

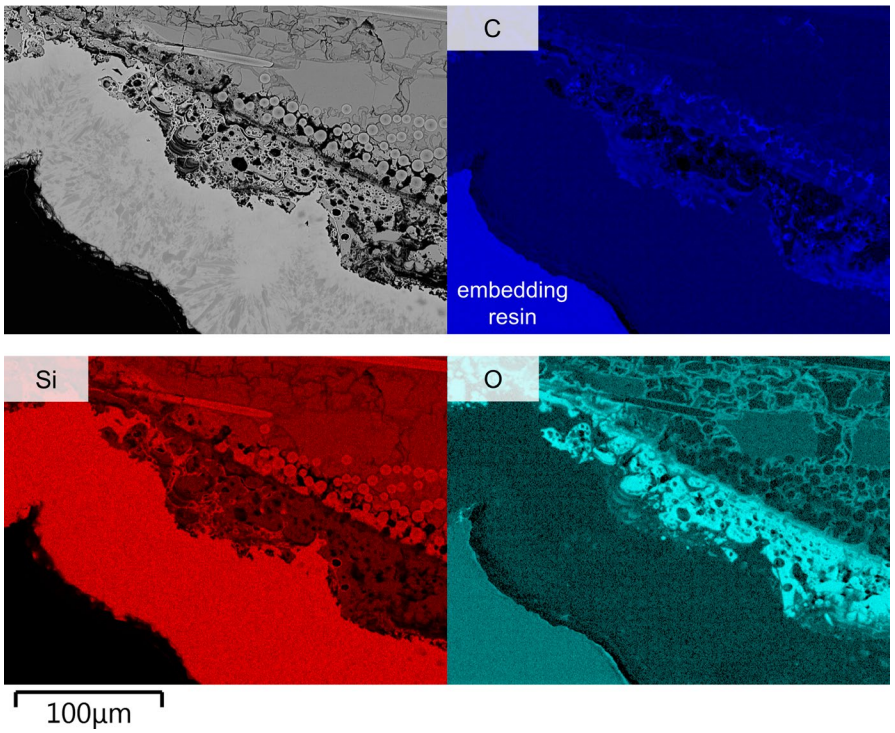

FIGURE 6 Spectrum analysis via EDX of cooling hole surface. EDX, energy dispersive X-ray spectroscopy [Color figure can be viewed at wileyonlinelibrary.com]

The foamy SiO_2 layer builds up via a chemical chain process at temperatures between 1470°C and 1527°C via following formulas ([22,33]):

$$SiC_{(s)} + O_{2(g)} \rightarrow SiO_{(g)} + CO_{(g)}$$

$$2SiO_{(g)} + O_{2(g)} \rightarrow 2SiO_{2(s)}$$

$$SiC_{(s)} + 2SiO_{2(s)} \rightarrow 3SiO_{(g)} + CO_{(g)}$$

SiC present in fiber and matrix is reacting with the atmosphere oxygen building gases that deposit as SiO_2. As SiO_2 reacts again with SiC, building other gases, gas bubbles are produced. Those bubbles are then trapped in the SiO_2 glassy phase at the end of laser machining, during cooling of the machined part. The SiO_2 glassy phase and bubbles inside this layer are emphasized via SEM analysis on Figure 5.

The hotter SiC/SiCN material during laser machining is, the better the porous SiO_2 layer builds up. Due to the laser beam inclination at 25°, about half of the inner surface of each cooling hole is longer exposed to the laser beam. Consequently, the SiO_2 layer only builds up on this surface as shown on Figure 7. The fiber orientation has also an influence on the local heat conductivity. With a higher thermal conductivity of the SA3 fibers (65 W/m at room temperature) compared to the SiCN

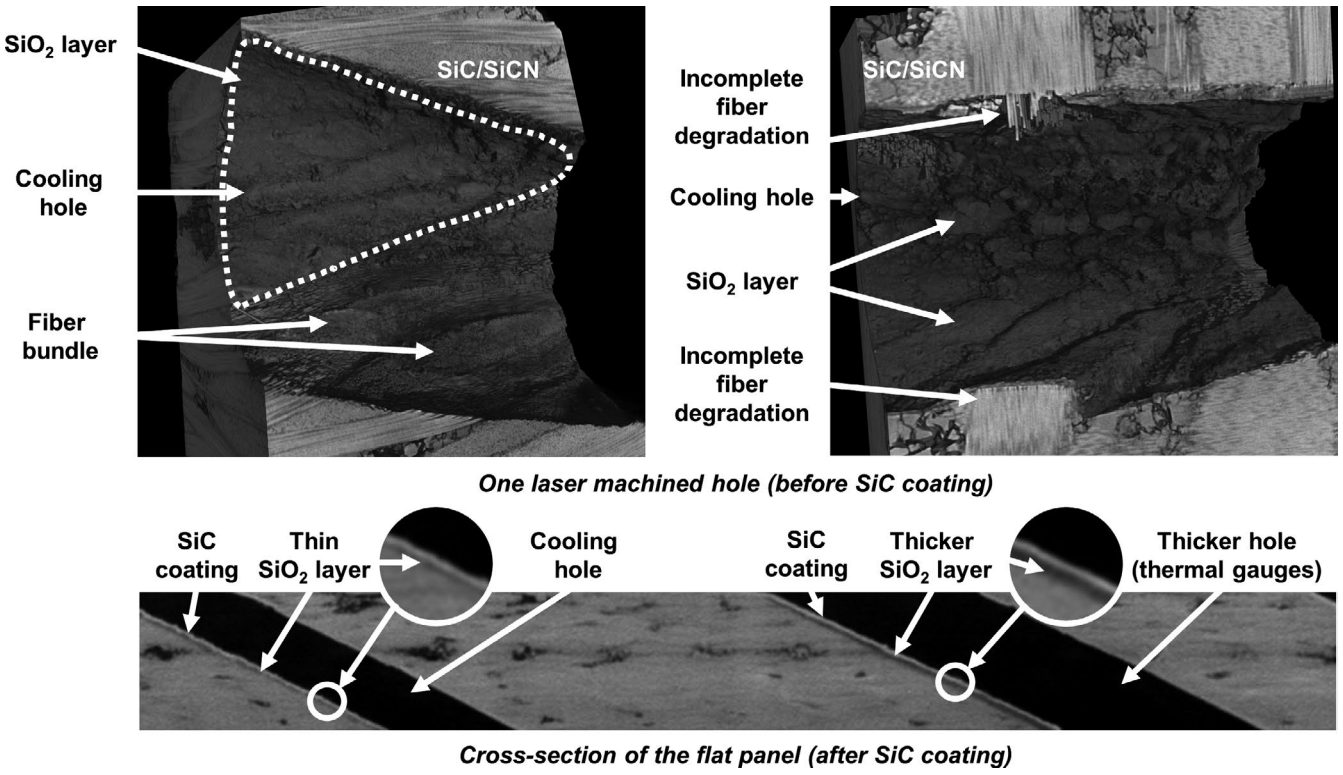

FIGURE 7 CT analysis of cooling holes before and after SiC coating process. CT, computing tomography

matrix ($\lambda_{\perp} \leq 3.1$ W/mK for comparable materials[22]), the parallelism between laser beam and fiber facilitates local heat propagation and therefore SiO_2 formation coupled with fiber/matrix degradation. On the contrary, incomplete fiber degradation is observed if the laser beam or the hole axis is transversal to fibers as shown on Figure 7. The heat concentration and therefore SiO_2 buildup is also enhanced with larger hole diameter, as observed for an instrumentation hole on the bottom of Figure 7. Amorphous SiO_2 has lower CTE and thermal conductivity than SiC/SiCN and SiC coating[34,35]:

$$SiO_2\text{:CTE} = 0.5 \times 10^{-6}/\text{K and } \lambda = 1.1 - 1.4\ \text{W/mK at room temperature}$$

$$\text{SiC:CTE} = 2.2 \times 10^{-6}/\text{K and } \lambda = 300\ \text{W/mK at room temperature}$$

$$\text{SiC/SiCN:CTE}_{//} = 1 \times 10^{-6}/\text{K and } \lambda_{//} = 18.3\ \text{W/mK at 50°C}$$

Therefore for long service at high temperature the SiO_2 phase will behave as local thermal isolator and reduce locally the cooling by conduction. This effect has though small impact on the overall cooling effectiveness. Nevertheless, cracks can occur in the SiC oxidative protection due to the different thermal expansions between the SiO_2 and SiC layers. So the buildup of the SiO_2 phase on the cooling hole has to be avoided for long-time application, either by using mechanical drilling technologies or other laser technology like a CO_2 laser. CO_2 laser machining might avoid SiO_2 build-up as shown by Lippmann on monolithic SiC.[19]

3.2 | HPCR evaluation

CT analysis previous to the cooling rig evaluation showed a macroscopic structure representative of the SiC/SiCN evaluated by Mainzer et al in Ref.[31] As the cooling effectiveness is measured on a macroscopic level, it can be assumed that measurement on one representative SiC/SiCN flat specimen is reproducible.

The pressure drop of a combustor and thus of the cooling air is an important parameter, because the pressure drop is the main driver for many processes, including, for example, liquid fuel atomization and mixing, affecting the overall combustor and engine performance. In consequence the pressure drop is not a free parameter with respect to the cooling design and its impact on the cooling performance has to be understood, especially for CMCs with different thermo-mechanical properties in comparison to conventional alloys.

In Figure 8 the total cooling effectiveness η_{tot} is shown for two different relative pressure drops of the cooling air (Δp_c). In the general level of cooling effectiveness there is only a small difference between $\Delta p_c = 4\%$ and $\Delta p_c = 2\%$. But there are differences in details that are important in combustor cooling

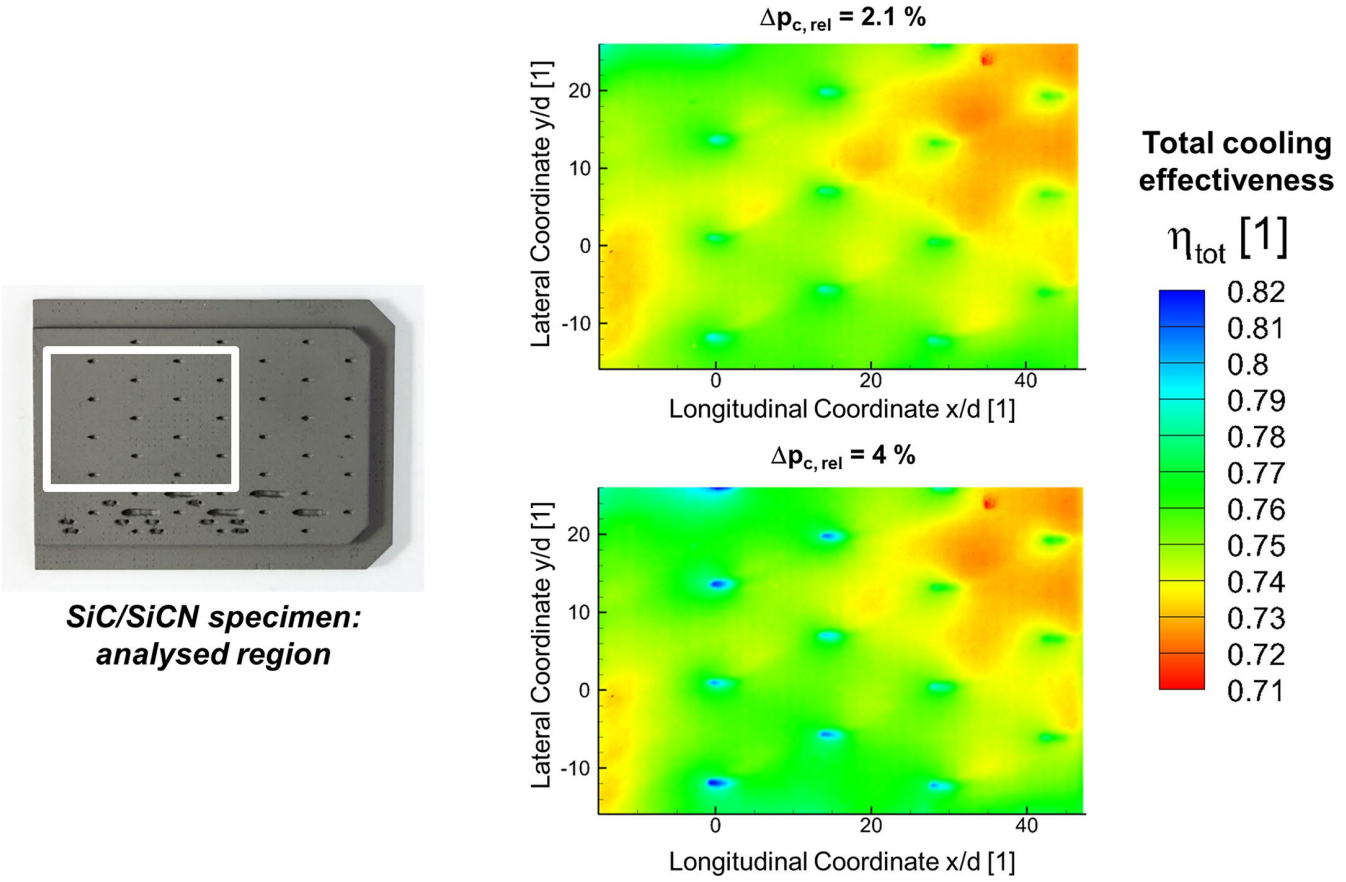

FIGURE 8 Cooling effectiveness of the SiC/SiCN specimen evaluated via combustor rig tests [Color figure can be viewed at wileyonlinelibrary.com]

applications. At $\Delta p_c = 4\%$ the cooling air flows with a velocity approximately 40% higher than for $\Delta p_c = 2\%$ through the effusion holes. The heat transfer coefficient increases proportional with the air velocity leading to an improved cooling in the vicinity of the effusion holes. This cooling mechanism is suitable to address radiative heat transfer from gases and soot. The holes can be identified by the colder spots (higher cooling effectiveness) especially at $x/d = 0$ or $x/d = 15$. But the increased cooling air velocity and the resulting increased cooling air mass flow does not lead to a significant improvement of the general level of the cooling effectiveness in comparison to $\Delta p_c = 2\%$. The high momentum of the cooling air jets at $\Delta p_c = 4\%$ leads to a jet lift of from the surface and hot gas from upstream may flow to the surface. At $\Delta p_c = 2\%$ the cooling air jets are more attached to the surface and the formed cooling air film is more efficient for convective heat transfer. The increased temperatures further downstream ($x/d > 25$) are attributed to an uncooled metal fixture of the CMC specimen. Due to limitations in the manufacturing route at this early stage, this solution had to be used.

For each individual combustor application the actual superposition of convective and radiative heat transfer has to be taken into account in order to design the correct cooling concept without any excessive cooling air consumption. The results shown in this contribution can be considered as a first feasibility study for more detailed investigations planned for the future.

The SiO_2 phase on the cooling hole face has no noticeable effect on the global cooling effectiveness. CT scans before and after rig tests reveal no modification of the macrostructure, the SiC coating kept intact, as the test duration was short (several hours). For a long-time application at high temperatures, the SiC coating might crack due to different thermal expansions of the SiC and SiO_2 layer. The formation of the SiO_2 layer has therefore to be avoided.

3.3 | Evaluation of MPI

The normalized MPI (MPI_{norm}) of the CMC SiC/SiCN and the alloys Inconel 718, HX and Haynes 282 are shown on Figure 9. The MPI of the alloys increase from room temperature up to a temperature range between 700°C and 800°C and then decrease rapidly while increasing temperature, mainly due to mechanical degradation. Inconel 718 and Haynes 282 show a high normalized MPI respectively up to 1 at 700°C and 0.7 at 760°C, whereas Inconel HX has a low normalized MPI up to around 0.2 at 800°C. At 1100°C Inconel 718

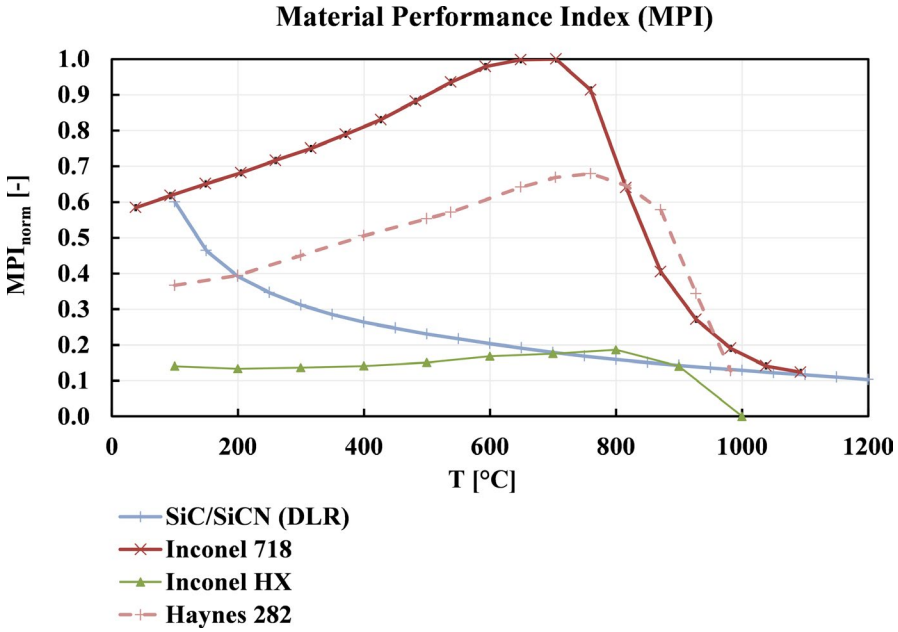

FIGURE 9 Normalized material performance index for different alloys and SiC/SiCN material [Color figure can be viewed at wileyonlinelibrary.com]

present the highest MPI of alloys with $MPI_{norm} = 0.12$; above this temperature the material might melt ($T_{melting} \geq 1260°C$).

The behavior of the MPI along temperature for SiC/SiCN is different: the normalized MPI continuously decreases from around 0.6 at room temperature up to a plateau of 0.1 at temperature above 1000°C. As explained previously in paragraph 2.4 only the minimal potential MPI for SiC/SiCN can be evaluated here, as the used thermal conductivities rely on literature values and are underestimated. The minimal MPI of SiC/SiCN remains constant above 1000°C, the potential of this CMC above 1000°C compared to nickel-base alloys is therefore emphasized. Thus SiC/SiCN composites are promising candidates for the service in cylindrical gas turbine components like combustors. In parallel to CMC development for combustor applications, efforts are being made worldwide to develop an oxidation stable coating for long time application.

One limitation of the presented MPI is the omission of fatigue and creep properties, which are other essential parameters for evaluating a material suitability for combustor components. Moreover the anisotropic nature of the CMCs should be taken into consideration while comparing them with their metallic counterparts. These topics are currently research points at the DLR and will be addressed in future publications.

4 | CONCLUSIONS

The machining effects via a ND-YAG laser in air on the microstructure and cooling effectiveness of a SiC/SiCN quasi-flat specimen were analyzed. Laser machining of 25° inclined holes leads to the buildup of a foamy SiO_2 layer on the surfaces exposed to the higher beam energy. The SiO_2 layer gets thicker if the machined hole diameter is bigger. An oxidative SiC layer coating can be applied even inner the machined holes and on the foamy SiO_2 layer. The cooling effectiveness of an effusive cooled SiC/SiCN flat panel coated with SiC was for the first time quantified and evaluated under specific rig test conditions at 0.76. The local SiO_2 layer has no significant effect on the overall cooling effectiveness. Though for long-time application at high temperatures, cracks might occur in the oxidative protection due to different thermal expansion between the SiO_2 layer on the cooling holes and the external SiC protective coating. The SiO_2 building can be avoided using other machining technologies like CO_2 laser or conventional diamond drilling. A MPI adapted to cylindrical components under thermal stresses is presented in this work. Whereas the index of typical combustor nickel-base alloys fall down above 800°C, SiC/SiCN shows a constant performance index above 1000°C. It shows the potential of SiC/SiCN CMCs above 1000°C compared to nickel-base alloys.

In future work DLR is developing further enhanced SiC/SiCN composites which will then being tested under realistic combustor environment.

ACKNOWLEDGMENTS

The authors thank Fiona Kessel, Rene Berres, Alberto Palomino, Tobias Schneider and Yuan Shi for their helpful support and technical assistance. The authors also thank all the technicians of the BT-KVS department at the DLR Stuttgart for their support in material manufacturing and machining.

ORCID

Sandrine Hönig https://orcid.org/0000-0003-1217-5396
Neraj Jain https://orcid.org/0000-0002-7853-1894
Thomas Behrendt https://orcid.org/0000-0002-4154-3277
Bernd Mainzer https://orcid.org/0000-0002-7358-492X
Dietmar Koch https://orcid.org/0000-0003-4504-8721

REFERENCES

1. Schulz E. Global networks, global citizens. Global market forecast 2018–2037. Airbus, editor. Blagnac Cedex F, editor. internet2018.
2. van Roode M. Ceramic gas turbine development: need for a 10 year plan. J Eng Gas Turbine Power. 2010;132(1):011301.
3. Corman GS, Luthra KL. 5.13 Development history of GE's prepreg melt infiltrated ceramic matrix composite material and applications. Compr Compos Mater II, 2018;325–38.
4. Behrendt T, Hackemann S, Mechnich P, Shi Y, Hönig S, Hofmann S, et al. Development and test of oxide/oxide ceramic matrix composites combustor liner demonstrators for aero-engines. J Eng Gas Turbine Power. 2017;139(3):031507.
5. Gerendás M, Wilhelmi C, Machry T, Knoche R, Werth E, Behrendt T, et al. Development and validation of oxide/oxide CMC combustors within the HiPOC program. ASME Turbo Expo 2013: Turbine Technical Conference and Exposition (GT2013). San Antonio, Texas, USA: American Society of Mechanical Engineers; 2013.
6. Foust M, Thomsen D, Stickles R, Cooper C, Dodds W. Development of the GE Aviation Low Emissions TAPS Combustor for Next Generation Aircraft Engines. 50th AIAA Aerospace Sciences Meeting including the New Horizons Forum and Aerospace Exposition. Nashville, Tennessee: AIAA; 2012.
7. Halbig M, Jaskowiak M, Kiser J, Zhu D. Evaluation of Ceramic Matrix Composite Technology for Aircraft Turbine Engine Applications. 51st AIAA Aerospace Sciences Meeting including the New Horizons Forum and Aerospace Exposition. Grapevine (Dallas/Ft. Worth Region), Texas: AIAA; 2013.
8. Vedula V, Shi J, Liu S, Jarmon DSector rig test of a ceramic matrix composite (CMC) combustor liner. In: Engineers ASoM, editor. ASME Turbo Expo 2006: Power for Land, Sea and Air. Barcelona, Spain: American Society of Mechanical Engineers; 2006. p. 255–9.
9. Bhatia T, Jarmon D, Shi J, Kearney S, Kojovic A, Hu J, et al. CMC Combustor Liner Demonstration in a Small Helicopter Engine. ASME Turbo Expo 2010: Power for Land, Sea and Air June 14-18, 2010; Glasgow, UK: American Society of Mechanical Engineers; 2010. p. 509–13.
10. GE9X Commercial Aircraft Engine. GE Aviation; 2019. [cited 2019 Nov 27]. https://www.geaviation.com/commercial/engines/ge9x-commercial-aircraft-engine
11. Chang CT, Lee C-M, Herbon JT, Kramer SK. NASA environmentally responsible aviation project develops next-generation low-emissions combustor technologies (Phase I). J Aeronaut Aerosp Eng. 2013;02(04):1000116. https://doi.org/10.4172/2168-9792.1000116
12. Padture NP. Advanced structural ceramics in aerospace propulsion. Nat Mater. 2016;15:804.
13. Guo S, Kagawa Y. Tensile fracture behavior of continuous SiC fiber-reinforced SiC matrix composites at elevated temperatures and correlation to in situ constituent properties. J Eur Ceram Soc. 2002;22(13):2349–56.
14. Katoh Y, Kotani M, Kishimoto H, Yang W, Kohyama A. Properties and radiation effects in high-temperature pyrolyzed PIP-SiC/SiC. J Nucl Mater. 2001;289(1-2):42–7.
15. Snead MA, Katoh Y, Koyanagi T, Singh GP. SiC/SiC materials handbook cladding properties. Oak Ridge, TN, USA: Oak Ridge National Lab. (ORNL); 2017. 2017–08-01. Report No.: ORNL/TM-2017/385. 100714.
16. Motz G, Schmidt S, Beyer S. The PIP-process: precursor properties and applications. In: Krenkel W, editor. Ceramic Matrix Composites: Fiber Reinforced Ceramics and their Applications. Germany, Weinheim: Wiley-VCH Verlag GmbH & Co. KGaA, 2008; p. 165–86.
17. Mainzer B, Lin C, Jemmali R, Frieß M, Riedel R, Koch D. Characterization and application of a novel low viscosity polysilazane for the manufacture of C- and SiC-fiber reinforced SiCN ceramic matrix composites by PIP process. J Eur Ceram Soc. 2019;39(2-3):212–21.
18. Markel IJ, Glaser J, Steinbrück M, Seifert HJ. Experimental and computational analysis of PSZ 10- and PSZ 20-derived Si-C-N ceramics. J Eur Ceram Soc. 2019;39(2-3):195–204.
19. Lippmann W, Knorr J, Wolf R, Reinecke A-M, Rasper R. Laser beam joining of non-oxidic ceramics for ultra high temperature resistant joints. 14th International Symposium on the Packaging and Transportation of Radioactive Materials (PATRAM 2004); September 20–24, 2004; Berlin, Germany; 2004.
20. Fu C, Yang Y, Huang Z, Liu G, Zhang H, Jiang F, et al. Investigation on the laser ablation of SiC ceramics using micro-Raman mapping technique. J Adv Ceram. 2016;5(3):253–61.
21. Li Z, Zhang F, Luo X, Chang W, Cai Y, Zhong W, et al. Material removal mechanism of laser-assisted grinding of RB-SiC ceramics and process optimization. J Eur Ceram Soc. 2019;39(4):705–17.
22. Herrmann M, Schönfeld K, Klemm H, Lippmann W, Hurtado A, Michaelis A. Laser-supported joining of SiC-fiber/SiCN ceramic matrix composites fabricated by precursor infiltration. J Eur Ceram Soc. 2014;34(12):2913–24.
23. Del Puglia P, Zonfrillo G. FEM study and optimisation of a CMC outer liner. Compos Struct. 2004;65(1):81–90.
24. Zonfrillo G, Giovannetti I, Manetti M. Material selection for high temperature applications. Meccanica. 2008;43(2):125–31.
25. Zhong F, Brown GL. Experimental study of multi-hole cooling for integrally-woven, ceramic matrix composite walls for gas turbine applications. Int J Heat Mass Transfer. 2009;52(3-4):971–85.
26. Mehta JM, Shouse D, Neuroth C, Marshall D, Cox B, editors. Multi-hole Film Cooling with Integrally Woven SiC-SiC Ceramic Wall Panels. ASME 2005 Summer Heat Transfer Conference collocated with the ASME 2005 Pacific Rim Technical Conference and Exhibition on Integration and Packaging of MEMS, NEMS, and Electronic Systems. San Francisco, California, USA: American Society of Mechanical Engineers Digital Collection; 2005.
27. Behrendt T, Hassa C. A test rig for investigations of gas turbine combustor cooling concepts under realistic operating conditions. Proc Inst Mech Eng, Part G: J Aerosp Eng. 2008;222(2):169–77.
28. Behrendt T, Lengyel T, Hassa C, Gerendás MS, editors. Characterization of Advanced Combustor Cooling Concepts Under Realistic Operating Conditions. ASME Turbo Expo 2008: Power for Land, Sea, and Air; 2008.
29. Timoshenko S. Thermal stresses in a long hollow cylinder. In: Timoshenko S, editor. Strength of materials, part II, 3rd ed. Toronto, Canada: D. Van Nostrand Company, Inc., 1956; p. 228–34.
30. Corman GS, Luthra KL. Silicon melt infiltrated ceramic composites (HiPerComp™). In: Bansal NP, editor. Handbook of ceramic composites. Boston, MA: Springer, US, 2005; p. 99–115.
31. Mainzer B, Frieß M, Jemmali R, Koch D. Development of polyvinylsilazane-derived ceramic matrix composites based on Tyranno SA3 fibers. J Ceram Soc Jpn. 2016;124(10):1035–41.
32. UBE Industries L. Tyranno Fiber® UBE Industries, LTD; 2020. [cited 2020 Jan 14]. https://www.ube.com/contents/en/chemical/continuous_inorganic_fiber/tyranno_fiber.html.

33. Shigematsu I, Kanayama K, Tsuge A, Nakamura M. Analysis of constituents generated with laser machining of Si3N4 and SiC. J Mater Sci Lett. 1998;17(9):737–9.
34. Filipovic L. Topography Simulation of Novel Processing Techniques. Technischen Universität Wien (University of Vienna): Technischen Universität Wien, Fakultät für Elektrotechnik und Informationstechnik; 2012.
35. Haas RA. CVD SILICON CARBIDE™. In: Haas RA, editor. 2008; p. 7.

How to cite this article: Hönig S, Süß F, Jain N, et al. Evaluation of preparation and combustion rig tests of an effusive cooled SiC/SiCN panel. *Int J Appl Ceram Technol*. 2020;17:1562–1573. https://doi.org/10.1111/ijac.13501